Parametric Interpretation of Trade-Wind Cumulus Budget Studies

ALAN K. BETTS

Department of Atmospheric Science, Colorado State University, Fort Collins 80523

(Manuscript received 2 January 1975, in revised form 17 June 1975)

ABSTRACT

This paper interprets the diagnostic budget studies of the undisturbed BOMEX period, 22–26 June 1969, using a parametric cloud model with continuous detrainment as well as entrainment. Compensating environmental motion, lateral detrainment and cloud transience are discussed in relation to the model results. The model shows the close coupling of the thermodynamic fluxes, and suggests that they can be represented well for some purposes, by a single cloud mass flux profile, rather than by a spectral cloud model. The extension of the methodology to precipitating convection is indicated briefly.

1. Introduction

Several papers have recently presented diagnostic budget studies of the undisturbed trade-wind cumulus layer—from BOMEX by Holland and Rasmussen (1973) and Nitta and Esbensen (1974), and from ATEX by Augstein *et al.* (1973). These have confirmed in more detail the importance of the cumulus transports in the maintenance of the trade-wind circulation, which was proposed in earlier papers (e.g., Riehl and Malkus, 1957). Further budget studies of this kind over a range of convective conditions and horizontal scales are being carried out during GATE (the GARP Atlantic Tropical Experiment). Quantitative convective budgets are fundamental to the development of numerical models for the tropical or global circulation, since these models must parameterize the convective transports and source terms which occur on scales unresolved by the numerical grid. In principle, the transports predicted by a parametric scheme need to be verified by comparison with transports derived from data, although this is not a simple task. It is necessary to generalize from a few observed case studies, and this requires a conceptual model of the convective transport processes for both the interpretation of the budget data and the construction of a parametric theory. Nitta (1975), for example, has used Arakawa's spectral cloud ensemble model (Arakawa and Schubert, 1974) to interpret the BOMEX budget data in terms of a model cloud population. In this model, each cloud type rises with a different entrainment rate, and detrains or spreads out into the environment at the level where it first reaches thermodynamic equilibrium.

The main purpose of this paper, which is a purely diagnostic study, is to show that the thermodynamic transports by the trade-wind cloud field can equally well, and perhaps more simply, be represented with a different conceptual model involving a single cloud type, which entrains and detrains at all levels during its life cycle. Budget data from the same BOMEX undisturbed period will be used to test this model. The fundamental asymmetry between the model concepts of entrainment and detrainment is discussed, and their relationship to the transience of individual clouds. A symmetric treatment of the coupled convective transports of sensible heat, water vapor and liquid water is proposed, which clarifies the significance of the convective flux of liquid water in both the thermal and water budgets. This requires a discussion of the thermodynamics appropriate to shallow moist convective systems.

2. Thermodynamics of non-precipitating convection

A useful starting point for the thermodynamics of shallow trade-wind clouds is to assume that the condensed liquid water is carried with the air as a parcel property. Betts (1973a) showed that the liquid water flux could then be combined with that of sensible heat through the definition of a new potential temperature (θ_L, a "liquid water potential temperature" analogous to θ_E, the equivalent potential temperature). This total θ_L flux was shown to be the significant vertical flux of enthalpy, which lead in the trade-wind case to regions of warming below and cooling above in the cumulus layer, as is observed. In this paper, we shall use static energies rather than potential temperatures. Betts (1974a) discusses the validity of this choice, and concludes that it is preferable to use static energy for budget calculations on convective fields which do not export kinetic energy. This seems

a good approximation for the trade winds. Hence, we shall derive the static energy analog of θ_L.

If the liquid water is carried with the air, then the reversible water saturation adiabat (Fjelstadt, 1925; Brunt, 1934) is the appropriate thermodynamic reference process. For a mixture of 1 gm of dry air and r gm of total water,

$$0=(C_p+rC)\frac{dT}{T}+d\left(\frac{Lr_s}{T}\right)-R_d\frac{dp_d}{p_d}, \tag{1}$$

where C_p, C, are the specific heats at constant pressure of dry air and liquid water, r_s, L are the saturation vapor mixing ratio and the latent heat of vaporization, and R_d, p_d are the gas constant and partial pressure of the dry air. A little exact manipulation using the Clausius-Clapyron equation and the hydrostatic equation for a model atmosphere having the vertical structure of the reversible adiabat (Betts, 1974a) yields

$$0=C_p'dT+d(Lq_s)+gdz_r, \tag{2}$$

where

$$\left.\begin{aligned} C_p'&=(C_p+rC)/(1+r)=\text{constant}\\ q_s&=r_s/(1+r)\end{aligned}\right\},$$

and z_r is the height in the model atmosphere above some reference, say 1000 mb. One can replace the water vapor in Eq. (2) by a liquid water term using

$$dr=0=dr_s+dr_l,$$

$$\frac{dL}{dT}=C_{pv}-C,$$

where r_l is the liquid water mixing ratio, and C_{pv} the specific heat of water vapor at constant pressure, to give

$$0=C_p''dT-d(Lq_l)+gdz_r, \tag{3}$$

where

$$\left.\begin{aligned} C_p''&=(C_p+rC_{pv})/(1+r)\\ q_l&=r_l/(1+r)\end{aligned}\right\}.$$

Eqs. (2) and (3) can be integrated explicitly (provided C_p and C_{pv} are taken as constants) since the mass of the system $(1+r)$ is constant, to define functions which are strictly conserved during the reversible water saturation process. However, practically, it is convenient to make two approximations

$$C_p''\approx C_p'\approx C_p,$$

$$z_r\approx z.$$

The first approximation is necessary because the atmosphere never has the model thermodynamic structure. The replacement of z_r which is the height calculated along the model reversible adiabat (on which the properties of the parcel lie) by z which is defined as the hydrostatic height of this parcel in a real atmosphere (which will, in general, not have this adiabatic structure) has a distinct physical meaning (see Betts, 1974a). It implies the neglect of the kinetic energy generation associated with the ascent of the parcel along the adiabat. For a thermal budget of a trade-wind layer, the export and time change of kinetic energy can be neglected, so that it is desirable to replace z_r by z, and by this means exclude any explicit computation of kinetic energy generation or dissipation. In contrast, if potential temperature θ were used for a thermal budget calculation, then to be exact, the generation of θ by the dissipation of kinetic energy must be included.

With these approximations, Eqs. (2) and (3) can be integrated to give two approximately conserved functions

$$h_s=C_pT+gz+Lq_s, \tag{4}$$

$$s_l=C_pT+gz-Lq_l. \tag{5}$$

The first is the saturation static energy, and the second we shall call the liquid water static energy as the analog of θ_L. (A suitable terminology is not obvious. The vertical flux of s_l represents the total thermal flux responsible for warming or cooling the atmosphere—see Section 3.) One way of conceiving these functions is to associate them with opposite-end states: $h_s>s$ because condensation of all the water vapor q_s will raise the static energy s of the parcel; whereas $s_l<s$ because evaporation of all the liquid water q_l will lower s.

For unsaturated air, they reduce to

$$h=C_pT+gz+Lq_v, \tag{6}$$

where q_v is the specific humidity, and

$$s=C_pT+gz, \tag{7}$$

defining the moist static energy and the static energy, respectively. These four functions are sufficient to discuss the thermodynamic transports by non-precipitating clouds: their analogous potential temperatures (see Betts, 1973a) are θ_{ES}, θ_L, θ_E and θ. We note that $Lq=h_s-s_l$ and $Lq_v=h-s$ so that the total water is specified by (h_s, s_l) for a saturated parcel and (h, s) for an unsaturated parcel. Note that h_s and s_l are clearly conserved in isobaric mixing (to the extent that we have approximated the specific heat by C_p, and taken L as a constant).

3. Budget equations

We can write budget equations for a non-precipitating cloud layer using the conserved variables h and s_l. For saturated regions of the layer h becomes h_s, while for unsaturated regions s_l becomes s. After

$\partial p \qquad \omega^* \partial p /$ convection cannot be parameterized solely in terms

averaging over a certain scale and neglecting horizontal eddy transports (following Yanai *et al.*, 1973), we obtain in pressure coordinates

$$\frac{\partial \bar{h}}{\partial t}+\bar{\mathbf{V}}\cdot\nabla\bar{h}+\bar{\omega}\frac{\partial}{\partial p}\bar{h}=Q_R-\frac{\partial}{\partial p}(\overline{\omega' h'}), \tag{8a}$$

$$\frac{\partial \bar{s}_l}{\partial t}+\bar{\mathbf{V}}\cdot\nabla\bar{s}_l+\bar{\omega}\frac{\partial}{\partial p}\bar{s}_l=Q_R-\frac{\partial}{\partial p}(\overline{\omega' s_l'}), \tag{8b}$$

where Q_R is the radiative source term. This pair of equations has a symmetric structure, and they yield on subtraction

$$L\left(\frac{\partial \bar{q}}{\partial t}+\bar{\mathbf{V}}\cdot\nabla\bar{q}+\bar{\omega}\frac{\partial \bar{q}}{\partial p}\right)=-L\frac{\partial}{\partial p}(\overline{\omega' q'}), \tag{8c}$$

where q is the *total* water. One further simplification of Eqs. (8b) and (8c) is possible: the neglect of variations on the large-scale of the mean liquid water content of the atmosphere; that is

$$\left.\begin{aligned}\delta\bar{s}_l &\approx \delta\bar{s}\\ \delta\bar{q} &\approx \delta\bar{q}_v\end{aligned}\right\}. \tag{9}$$

Generally, this will be an excellent approximation on the left-hand side of Eqs. (8b) and (8c) for the trade wind layer, because the time change of liquid water storage will typically be small, and the mean liquid water content is negligible in the advective terms. Eq. (9) does require that in the mean the layer remains unsaturated. This approximation is also necessary if we are to proceed with the interpretation without measurements of the mean liquid water content $\bar{q}_l$. Eqs. (8b), (8c) and (8a) then become

$$Q_1=\frac{\partial \bar{s}}{\partial t}+\mathbf{V}\cdot\nabla\bar{s}+\bar{\omega}\frac{\partial}{\partial p}\bar{s}=Q_R-\frac{\partial}{\partial p}(\overline{\omega' s_l'}), \tag{10b}$$

$$-Q_2=L\left(\frac{\partial \bar{q}_v}{\partial t}+\bar{\mathbf{V}}\cdot\nabla\bar{q}_v+\bar{\omega}\frac{\partial \bar{q}_v}{\partial p}\right)=-L\frac{\partial}{\partial p}(\overline{\omega' q'}), \tag{10c}$$

$$Q_1-Q_2=\frac{\partial \bar{h}}{\partial t}+\bar{\mathbf{V}}\cdot\nabla\bar{h}+\bar{\omega}\frac{\partial \bar{h}}{\partial p}=Q_R-\frac{\partial}{\partial p}(\overline{\omega' h'}), \tag{10a}$$

where Q_1, Q_2 are the apparent heat source and water vapor sink as defined by Nitta (1972) and Yanai *et al.* (1973), and are the basic quantities that can be derived by budget calculations from the large-scale thermal and water vapor fields. The eddy transport terms on the right-hand side will be interpreted as convective transports. Eq. (10a) has been widely used (Yanai *et al.*, 1973; Ogura and Cho, 1973; Nitta and Esbensen, 1974) since it does not contain the troublesome liquid water storage or liquid water fluxes (which are usually written as an unknown source term: the difference between condensation and evaporation at a level). However, two of these three equations are necessary to specify the nature of the convective thermodynamic fluxes. One can derive and discuss the flux of $\overline{\omega' s_l'}$ in an analogous manner to $\overline{\omega' h'}$ provided the assumption is made that liquid water is carried with the air. [For precipitating systems, the vertical fluxes of static energy and liquid water cannot be combined to a single flux, but they must still be handled as coupled fluxes (see Section 8).] The use of s_l as a variable will correctly describe both condensation and the evaporation process associated with mixing between cloud and unsaturated environment. Indeed the flux $\overline{\omega' s_l'}$ in Eq. (10b) should be regarded as the total thermal transport by the clouds (see below). Eq. (10c) is important because it shows that the convective flux derived from Q_2 is the total water flux (liquid plus vapor) carried by the clouds. This has not always been clear in earlier papers (e.g., Holland and Rasmusson, 1973).

Three fundamental convective fluxes can thus be defined (for convenience, upward fluxes have been defined as positive):

$$F_h=-\overline{\omega' h'}=\int_0^p (Q_1-Q_2-Q_R)dp \tag{11a}$$

$$F_{s_l}=-\overline{\omega' s_l'}=\int_0^p (Q_1-Q_R)dp \tag{11b}$$

$$F_{Lq}=-L\overline{(\omega' q')}=-\int_0^p Q_2 dp. \tag{11c}$$

Only two of these are independent, since $F_h=F_{s_l}+F_{Lq}$. F_h can be computed without any assumptions on $\bar{q}_l$. If large-scale mean changes of $\bar{q}_l$ are observed, one can generalize Q_1, Q_2 to become the large-scale sources, sinks of $\bar{s}_l$, $\bar{q}$. Further, as mentioned above, one can generalize F_{s_l}, F_q for precipitating convection to become the mean vertical small-scale flux of $s-Lq_l$, q_v+q_l, even though the precipitation is falling independently of the air (see Section 8).

In all cases, the slope of these flux curves (e.g., Figs. 1 and 7) is related to the convective warming and cooling, drying and moistening of the mean atmosphere. These are the fluxes which can be derived from diagnostic budget data (see Section 5 and Fig. 1). They are coupled fluxes. One cannot derive, for example, the separate fluxes of static energy or liquid water without the use of a specific transport model or "cloud model." The next section introduces such a model. However, since the liquid water static energy flux F_{s_l} is the least familiar of the three, it is worth commenting on its significance here. The use of a simple entraining cloud model (see also Betts, 1973a) shows F_{s_l} is dominated by the cloud liquid water flux $\overline{L\omega' q_l'}$ (see Fig. 2). Small entraining cumulus

clouds condense liquid water at one level, transport it upward, and reevaporate this liquid water at a higher level. This evaporative cooling is the process which (together with the radiative cooling) maintains the trade inversion against the warming produced by large-scale subsidence.

4. Parameterization of the fluxes F_{sl}, F_{Lq}, F_h

These fluxes can be derived using Eqs. (10) and (11) from large-scale budgets for a trade-wind layer. We shall show, using the BOMEX data, that they can be represented parametrically by the product of a single convective mass flux (ω^*) and a perturbation quantity derived from a single entraining cloud parcel (suffix c) rising through the known mean environment, namely

$$F_h=-\overline{\omega' h'}\equiv\omega^*(h_{sc}-\bar{h}), \tag{12a}$$

$$F_{sl}=-\overline{\omega' s_l'}\equiv\omega^*(s_{lc}-\bar{s}), \tag{12b}$$

$$F_{Lq}=-L\overline{\omega' q'}\equiv L\omega^*(q_c-\bar{q}_v). \tag{12c}$$

The mean environment here is taken as unsaturated. Note that ω^* has been defined as positive. Parameterization of the fluxes in this way has been used in several papers (e.g., Ooyama, 1971; Betts, 1973a; Yanai *et al.*, 1973). There are several important general consequences of this method of parameterization. The large-scale modification rate produced by the convection is given by [taking Eq. (11a) as example]

$$Q_1-Q_2-Q_R=\frac{\partial}{\partial p}(F_h)=\frac{\partial}{\partial p}[\omega^*(h_{sc}-\bar{h})]$$

$$=-\omega^*\frac{\partial h}{\partial p}+\omega^*\frac{\partial h_{sc}}{\partial p}+(h_{sc}-\bar{h})\frac{\partial\omega^*}{\partial p}.$$

Now if we define an entrainment rate for an ascending cloud parcel as $\lambda(>0)$, then

$$\frac{\partial h_{sc}}{\partial p}=\lambda(h_{sc}-\bar{h}), \tag{13}$$

with similar equations for s_{lc}, q_c, and we may write

$$Q_1-Q_2-Q_R=-\omega^*\frac{\partial\bar{h}}{\partial p}+\omega^*(h_{sc}-\bar{h})\left(\lambda+\frac{1}{\omega^*}\frac{\partial\omega^*}{\partial p}\right). \tag{14a}$$

Similarly, with the approximation $\bar{s}_l\approx\bar{s}$, we have

$$Q_1-Q_R=-\omega^*\frac{\partial\bar{s}}{\partial p}+\omega^*(s_{lc}-\bar{s})\left(\lambda+\frac{1}{\omega^*}\frac{\partial\omega^*}{\partial p}\right), \tag{14b}$$

and with $\bar{q}\approx\bar{q}_v$,

$$-Q_2=-L\omega^*\frac{\partial\bar{q}_v}{\partial p}+L\omega^*(q-\bar{q}_v)\left(\lambda+\frac{1}{\omega^*}\frac{\partial\omega^*}{\partial p}\right). \tag{14c}$$

This manipulation of the convective flux divergence shows that the parameterization represented by Eq. (12) is equivalent to an apparently different model. In Eq. (14), the first term can be interpreted as the parameterization of the convective change in terms of the additional subsidence of the environment forced by the convection; since

$$\bar{\omega}=(-\omega^*)+(1-\alpha)\omega(e),$$

therefore,

$$\omega(e)\approx\bar{\omega}+\omega^*,$$

if α, the fractional area of convection, is small. We see that if the second term in Eq. (14) vanishes, then this "subsidence term" is the only convective effect. This will be the case if

$$\frac{1}{\omega^*}\frac{\partial\omega^*}{\partial p}=\lambda,$$

that is, if the cloud mass flux increases upward at the entrainment rate. The spectral cloud model of Arakawa and Schubert (1974) satisfies this condition up to the detrainment level where ω^* goes rapidly to zero. However, one may propose a more general model by introducing the concept of continuous detrainment with height (averaged over a cloud life cycle—see later). Then we may define a reciprocal scale length for detrainment as

$$\mu=\lambda+\frac{1}{\omega^*}\frac{\partial\omega^*}{\partial p}. \tag{15}$$

The second term in Eq. (14) is then interpreted as the effect of detrainment of cloud mass with properties differing from that of the environment. Thus, a general flux parameterization of the type of Eq. (12) includes the effects both of "compensating subsidence" and "lateral detrainment" of cloud mass (as in Kuo, 1965). Ooyama (1971) used a similar model to describe cumulus convection in terms of a population of entraining and detraining bubbles. This relationship was related by Fraedrich (1973) to cloud transience, to which we will return later. Betts (1973b) used essentially the same formulation in a cumulonimbus budget study. Kuo (1974) has disputed the interpretation of convective heating in terms of cloud-induced subsidence. However, the derivation above clearly shows that the divergence of convective heat flux parameterized by Eqs. (12) can be split up, and the first term interpreted in this manner. Only the second term represents a detrainment of cloud properties at a certain level, and it does not seem logically possible to permit detrainment in a layer (represented by $\mu>0$) without having a mass flux $\omega^*(p)$ up to that level.

Conversely, this analysis also shows that cumulus convection *cannot* be parameterized solely in terms

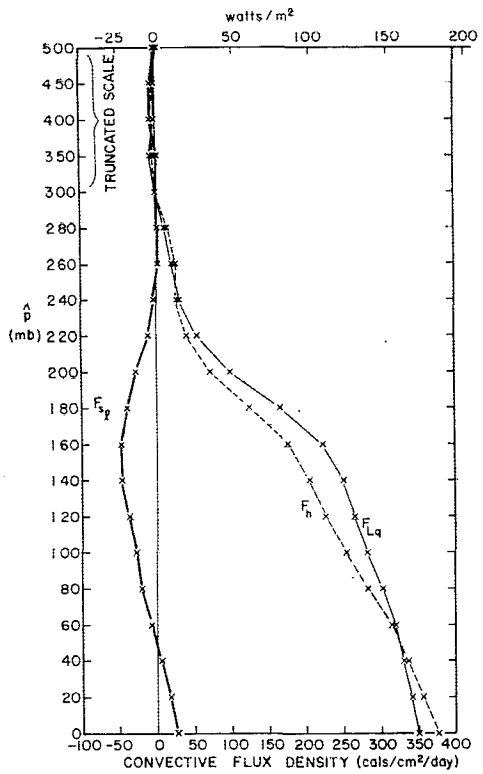

FIG. 1. Vertical convective fluxes of moist static energy, total water substance, and liquid water static energy for the BOMEX undisturbed period, 22–26 June 1969.

of a mass flux or the equivalent compensating motion of the environment. One important conclusion is that Eq. (46) of Betts (1973a) which was used to close a subcloud-layer model is incorrect. Betts (1973a) parameterized the cloud-base (suffix B) convective heating rate as (using this paper's notation)

$$(Q_1-Q_R)_B=-\omega_B^*\frac{\partial\bar{s}}{\partial p}.$$

This should be

$$(Q_1-Q_R)_B=-\omega_B^*\left[\frac{\partial\bar{s}}{\partial p}-\mu(s_{lc}-\bar{s})\right]. \tag{16}$$

In my original paper (Betts, 1970), the detrainment term was included in the corresponding water vapor equation (where it dominates) but omitted from the thermal equation. However, in Section 7, we shall show that the second term in Eq. (16) is typically a third of the magnitude of the first and of opposite sign, and hence, not negligible. Formally the detrainment term in Eq. (16) can only become zero if $(s_{lc}-\bar{s})$ and hence F_{s_l} both go to zero. This is not generally the case even at cloud base, since although $s_{lc}\to s_c$ as cloud $q_l\to 0$, typically $(s_c-\bar{s})$ and F_{s_l} remain negative, and the detrainment term remains significant because μ is large. The use of the correct Eq. (16) adds an additional term to the cloud-base boundary condition [Eq. (50) of Betts (1973a)]. The incomplete equation has been used by later papers (e.g., Hoeber, 1973; Sarachik, 1974).

5. Application to BOMEX undisturbed period: 22–26 June 1969

A number of authors have presented diagnostic studies based on this 5-day undisturbed period (Holland and Rasmusson, 1973; Nitta and Esbensen, 1974). Fig. 1 shows the convective fluxes computed using Eqs. (11) and data kindly supplied by Nitta and Esbensen, and Cox (1973). All these curves have appeared previously, although separately, with some confusion over their interpretation. Holland and Rasmussen (1973) showed F_q (although they interpreted it as F_{qv}), Nitta and Esbensen (1974) showed F_h, and Betts (1973a) showed F_{s_l} (labelled as a convective enthalpy flux). Fig. 1 summarizes the interrelations between all three fluxes.

The Q_1 and Q_2 data used in the computation are a little noisy above $\hat{p}=300$ mb ($\hat{p}$ is pressure below the surface pressure) but most of the variations disappear in the 5-day average. The 5-day mean fluxes were therefore set at zero at $\hat{p}=300$ mb since in the mean they remain essentially zero from $\hat{p}=300$ to 500 mb (see Fig. 1). The resulting mean F_h curve differs slightly from that shown by Nitta and Esbensen (1974), since they made small corrections to the Q_1, Q_2 data at the upper levels and also used preliminary radiation data supplied by S. K. Cox. The final BOMEX radiation data (Cox, 1973) were computed using sounding data and observed cloud distributions to give daily average values of the net radiative cooling rate (shortwave and longwave) for 50 mb layers. This paper uses the cooling rates averaged for the 5 days, 22–26 June.

In Fig. 1, the F_{s_l} curve shows the region of convective warming below $\hat{p}=160$ mb and cooling above; and the F_{Lq} and F_h curves show the addition of water vapor and moist static energy at all levels, with the largest additions in the trade inversion layer (see Figs. 2 and 5). The observed cloud base was about $\hat{p}=65$ mb (Holland and Rasmusson, 1973; Esbensen, 1975).

Fig. 2 shows the profiles of $\bar{s}$, $\bar{h}$, $\bar{h}_s$ for the mean environment and s_{lc}, h_{sc} (solid lines) for an ascending parcel for different entrainment rates $\lambda=0$, 0.002, 0.005, 0.010. It is necessary to assume some initial value for s_{lc}, h_{sc} at cloud base to integrate Eq. (13). Since s_{lc} is very small at cloud base and cannot be determined accurately from the data, we chose cloud base values which corresponded to saturation at $\hat{p}=65$ mb, but also gave the same cloud base mass fluxes ω^* in Eqs. (12a), (12b). That is, agreement of the mass flux values in Fig. 3 was imposed at cloud

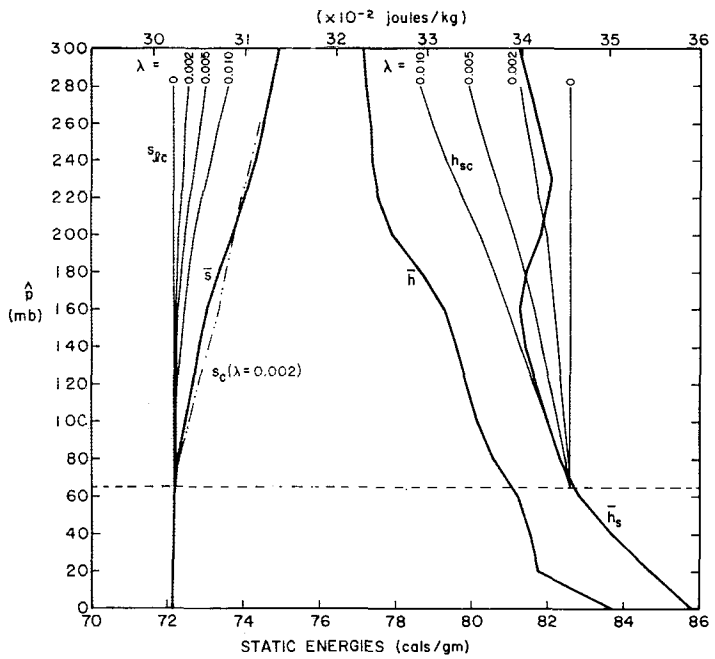

FIG. 2. Mean environmental profiles of static energy, moist static energy, saturation static energy, and cloud parcel ascent paths for different entrainment rates for the same BOMEX undisturbed period.

base. The resulting s_{lc} at cloud base is extremely close to the mixed layer value, while h_{sc} is slightly moister than the mixed layer mean. This suggests that air rising from the subcloud layer to form clouds is a little moister than the mean mixed layer, which is in general agreement with observation (e.g., Betts *et al.*, 1974).

Fig. 3 shows the $\omega^*(\hat{p})$ curves calculated from the F_h and F_{s_l} fluxes using Eqs. (12) and (13). Only two values of λ are shown for clarity; the curves change

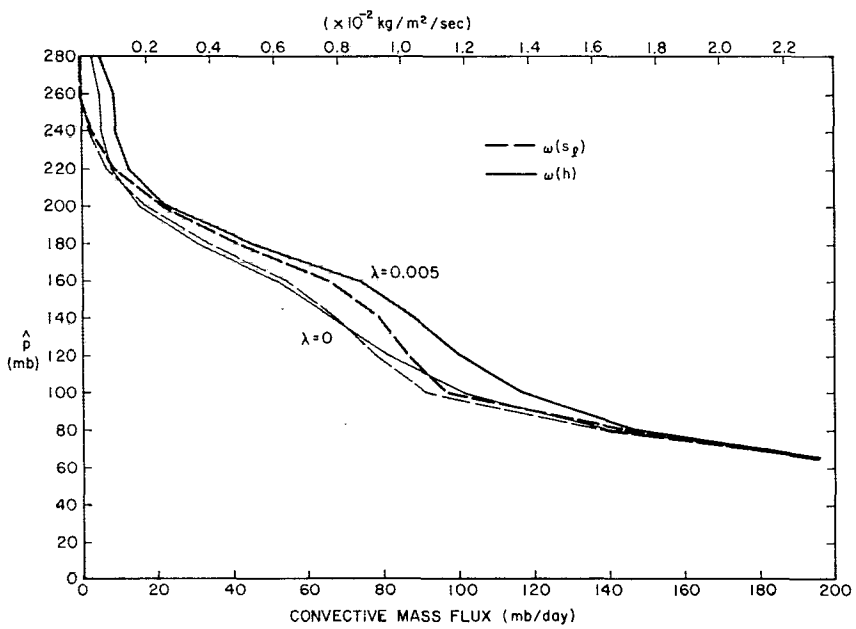

FIG. 3. Derived convective mass flux profiles for the BOMEX undisturbed period for two values of an entrainment parameter.

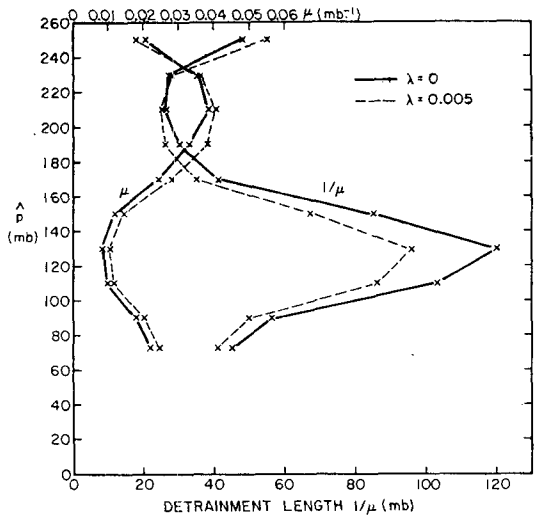

FIG. 4. Vertical variation of detrainment for two values of entrainment.

uniformly with changing λ. The ω^* curve derived from F_{Lq} is essentially identical to that derived from F_h. For $\lambda=0$, the pairs of curves are essentially identical although they diverge slowly for increasing λ. It appears that the observed convective transports can be represented by a single mass transport curve $\omega^*(\hat{p})$ using any small value of λ. The fit is best for $\lambda=0$, but considering the probable errors in the data, quite satisfactory for values of $\lambda<0.005$. Larger values of λ would not make much sense in this model, since conceptually we require a cloud parcel to rise through the whole cloud layer, even though we are not actually using a kinetic energy equation in this model. From Fig. 2, it is clear that with $\lambda\gtrsim0.005$, a cloud parcel would have insufficient buoyancy to rise through the inversion, even allowing for some overshoot.

The significance of Fig. 3 is that it shows the close coupling of the heat and water transports, a result which is of vital importance to the successful parameterization of these fluxes. It also shows that a simple model (that is, even one with no entrainment or a single value of λ) may well describe the transports with sufficient accuracy. Although agreement of the curves was imposed at 65 mb by choosing cloud-base values of s_{lc}, h_{sc}, this does force agreement of the curves above cloud base. [If the reverse assumption is made, namely that the ω^* profiles are *chosen* the same, then one can derive in-cloud properties as a function of height, as, for example, in Yanai *et al.* (1973).]

Fig. 2 also shows (dot-dashed line) the cloud parcel static energy s_c for $\lambda=0.002$. This curve is uniquely related to h_{sc}, but it enables one to partition $(s_{lc}-\bar{s})$ into $(s_c-\bar{s})$ and $-Lq_{lc}=s_{lc}-s_c$. Multiplying by ω^* from Fig. 3, we then partition F_{s_l} into the separate fluxes of static energy

$$F_s=\omega^*(s_c-\bar{s}),$$
$$-F_{Lq_l}=-\omega^*Lq_l=\omega^*(s_{lc}-s_c).$$

Over most of the layer (65–210 mb for $\lambda=0.002$) F_s is upward, associated with positive buoyancy, and much smaller than $-F_{Lq_l}$ which is downward and associated with an upward liquid water flux. Thus F_{s_l} is dominated by the liquid water flux. From Fig. 2, one can see that the buoyancy $(s_c-\bar{s})$ and associated F_s remain small because the cloud parcel is rising through a stably stratified atmosphere, while cloud liquid water which is carried with the parcel and the associated F_{Lq_l} increase with height.

Fig. 4 shows the variation of the detrainment as a function of height for $\lambda=0$ and 0.005. It shows detrainment large just above cloud base and in the inversion layer. Thus, the model predicts a detrainment rate μ which is much larger than and nearly independent of the entrainment rate λ (for realistic values of λ). Indeed, λ can be zero, but detrainment is still important. Figs. 3 and 4 raise the question of the physical interpretation of the $\omega^*(\hat{p})$ curve, and these large detrainment values. This is the subject of Section 6.

One could identify three distinct convective layers in Fig. 1: the subcloud layer ($\hat{p}<65$ mb), the lower cloud layer ($65<\hat{p}<160$ mb) which is warmed and moistened by the convection, and the upper cloud or inversion layer ($160<\hat{p}<240$ mb) which is cooled and moistened by the convection. The upper boundary of the convection is not distinct in this average, but the region of cooling by the convection corresponds closely to the more stable layer, identifiable in Fig. 2 as the layer where h_s increases with height. It is illustrative to look at the convective and radiative budget terms for these three layers as shown in Fig. 5. (The residual fluxes above 240 mb have been ignored.) The convective terms were derived using Eq. (10) as residuals of the large-scale time change and advective terms and the radiative term. Of the large-scale terms, the advection terms dominate and, in particular, the mean vertical advective term produced by the large-scale subsidence (see Holland and Rasmusson, 1973). Thus, in the upper cloud layer, the radiative and convective cooling are balanced primarily by the large-scale subsidence warming, while in the lower cloud layer it is the radiative cooling which closely balances the convective heating and large-scale advective changes. In the subcloud layer the radiative cooling and convective heating themselves closely balance. The resulting balanced structure changes only slowly in time.

In a diagnostic study, we only derive the convective fluxes from the large-scale parameters. In fact, the radiative and convective fluxes are themselves coupled—in Fig. 5 the radiative fluxes (from Cox, 1973)

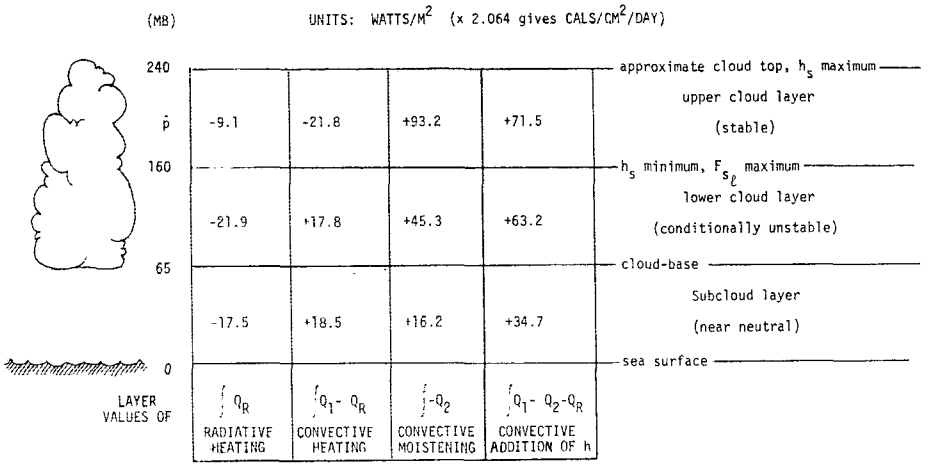

FIG. 5. Radiation and convection source terms for the three convective layers.

have been deduced from the observed thermodynamic profiles and cloud fields.

One further breakdown of the convective sources is of interest. Table 1 presents for $\lambda=0$ the decomposition of Q_1-Q_R, $-Q_2$ and $Q_1-Q_2-Q_R$ into the two separate terms in Eq. (14): the large-scale changes produced by induced environmental subsidence and by detrainment of cloud air to the environment. We see that in the thermal balance, the subsidence term dominates in the lower cumulus layer corresponding to the region of convective warming in Figs. 1 and 5 while, in the more stable upper layer (the trade inversion), the detrainment of s_l (liquid water static energy) dominates, resulting in the layer of cooling. However, in the water and moist static energy balances, the detrainment term dominates at all levels, resulting in the input of water vapor and moist static energy to the mean atmosphere. We see that just above cloud base the detrainment term in Eq. (16) is not negligible. It should be emphasized, however, that this is a breakdown of the parametric model; the effect of the convection on the mean atmosphere remains always the sum of the two terms.

6. Detrainment and cloud transience

If $\lambda=0$ in Eq. (15), then the slope of the curve in Fig. 3 gives

$$\mu=\frac{1}{\omega^*}\frac{\partial\omega^*}{\partial p}.$$

Thus, the model and the data imply that even though entrainment may be small or zero, μ is not. Fig. 4 showed a profile of μ.

This concept of detrainment as parameterized in Eq. (14) is essentially distinct from entrainment, because the two processes have been modeled on different time scales. The *entrainment* into a cloud has been considered as a process on the cloud time scale, which affects the properties of the cloud [Eq. (13)]. However, the *detrainment* to the environment affects the environment only on the time scale of the environment, that is, of the mean large-scale changes [Eqs. (14) and (10)].

In the real atmosphere clouds grow to some height and then decay setting up a reverse downward circula-

TABLE 1. Decomposition of convective source terms (W m^{-2}) into compensating environmental subsidence and lateral detrainment [Eq. (14)].

Layer (mb)	$\omega^*\Delta\bar{s}$	$-\Delta\omega^*(s_{lc}-\bar{s})$	Sum	$\omega^*\Delta\bar{h}$	$-\Delta\omega^*(h_{sc}-\bar{h})$	Sum	$\omega^*L\Delta\bar{q}$	$-\Delta\omega^*L(q_{sc}-\bar{q})$	Sum
65-80	7.0	-2.7	4.3	−39.1	50.5	11.4	−46.1	53.2	7.1
80–100	9.9	−5.5	4.4	−25.1	39.2	14.2	−35.2	44.9	9.7
100-120	6.9	−2.7	4.3	−13.6	26.4	12.8	−20.9	29.4	8.5
120–140	6.4	−2.8	3.6	−9.6	20.5	10.9	−16.0	23.4	7.3
140–160	6.5	−5.1	1.3	−9.0	23.0	13.9	−15.4	28.0	12.5
160-180	6.9	−10.4	−3.5	−12.6	37.3	24.7	−19.4	47.8	28.4
180–200	4.9	−11.4	−6.5	−8.2	33.9	25.7	−12.8	45.1	32.3
200–220	2.0	−9.1	-7.1	−2.5	17.4	15.0	−4.3	26.2	21.9
220–240	0.5	−5.0	−4.5	−0.6	6.6	5.9	−1.3	12.0	10.7
240–260	0.1	−2.0	−2.0	−0.1	1.6	1.4	−0.5	4.1	3.6

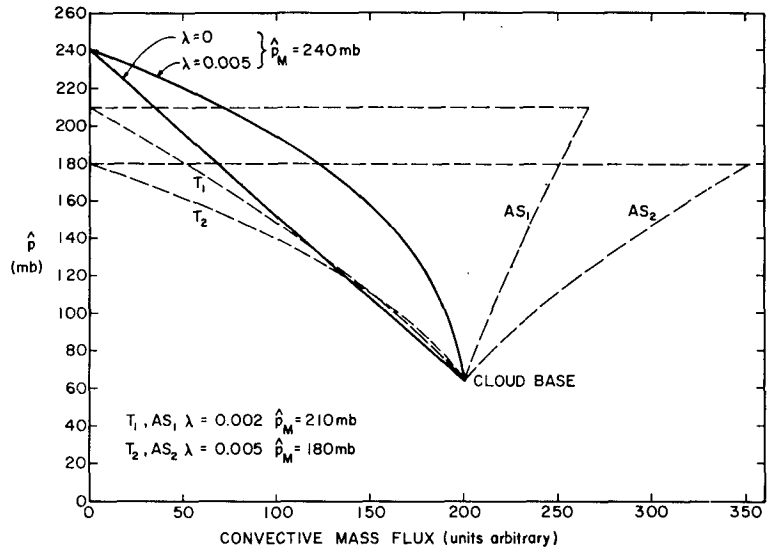

FIG. 6. Schematic cloud mass flux profiles for transient cloud model with $\hat{p}_M$ [Eq. (17)]=240 mb (solid line). Comparison of transient cloud model (T) mass flux with Arakawa and Schubert model (1974), denoted AS (dashed lines).

tion, with presumably a series of oscillations before some equilibrium state is reached when what was cloud now becomes part of the new environment (modified by mixing and vertical circulations). However the model represented by Eqs. (12)–(14) considers only an upward circulation with the continuous detrainment of cloud mass flux to the environment. Because the model environment is considered uniform, this implied detrained cloud air is rapidly mixed with the environment, which only changes slowly on the time scale of the large-scale fields. This separation of time scale is basic to the concepts of cloud and environment as used in parametric models. It is valid provided the fractional area cover of cloud is small (see Betts, 1973a, 1974b; Yanai *et al.*, 1973; Arakawa and Schubert, 1974). The main difference between a model with continuous detrainment and one with a reverse decay circulation is that detrainment at a level modifies the environment only at that level, while a circulation can spread the modification over a deeper layer.

The model used in this paper could be regarded as a type of transient cloud model. For example, consider a cloud that grows without entrainment from cloud base $\hat{p}_B$ to a maximum pressure height $\hat{p}_M$ at a uniform rate with uniform cloud base mass flux ω^*_B. Let it then at once decay, become inactive, and be rapidly mixed with the environment or detrain. The mean vertical mass flux over this life cycle is

$$\omega^*(\hat{p})=\left(\frac{\hat{p}_M-\hat{p}}{\hat{p}_M-\hat{p}_B}\right)\omega^*_B. \tag{17}$$

That is, a cloud undergoing this life cycle of growth and rapid decay results in a *linear* decrease with pressure ($\hat{p}$) of $\omega^*(\hat{p})$ over its life cycle (Fig. 6). The addition of entrainment only adds a multiplying factor of $\exp\lambda(\hat{p}-\hat{p}_B)$ to this profile.

The solid lines in Fig. 6 are two such profiles for $\lambda=0$ and $\lambda=0.005$, both with $\hat{p}_M=240$ mb, roughly corresponding with the top of the cloud layer. These simple model profiles, based on a uniform cloud-base mass flux and cloud growth, while explaining the general decrease of ω^* with height, do not agree closely with the derived $\omega^*(\hat{p})$ profiles in Fig. 3, because the initial decrease of ω^* with height is too steep. Clearly, therefore, one could further interpret the Fig. 3 ω^* profiles as the sum of different cloud types. However it may be possible even in a predictive model to predict the $\omega^*(\hat{p})$ profile for small clouds directly from some quasi-equilibrium assumption.

The dashed lines in Fig. 6 show a comparison of this simple transient cloud model, denoted T, with the cloud model of Arakawa and Schubert (1974), denoted AS. For the comparison we have chosen $p_M(\lambda)$ corresponding to the level where $h_{sc}(\lambda)=\bar{h}_s$ in Fig. 2, which is the detrainment level of Arakawa and Schubert (neglecting the virtual temperature correction). If a spectral cloud model is used, then it may be more economical to construct the convective transports from functions of the type T rather than the type AS, at least for the shallow cloud population. For the transient cloud model, it is not necessary to choose $p_M(\lambda)$ at the thermal equilibrium level as in Fig. 6; a simple kinetic energy equation could be used to predict the maximum cloud height reached.

7. Comparison with other papers

It was mentioned in Section 5 that the curves in Fig. 1 have been published previously, albeit separately. Nitta (1975) has derived cloud mass flux distribution curves using a spectral model for the same period. These are similar to Fig. 3. One might think that the cloud-base mass flux would be a simple quantity to compare: however, ω^* (my notation) or M_c (Nitta, 1975) is rapidly changing near cloud base, and as a derived parameter is also very sensitive to the choice of cloud-base properties. Nitta chose $\hat{p}=60$ mb as the top of the mixed layer for this undisturbed period, while I have chosen 65 mb as cloud base. Further, Nitta used mixed layer properties to define (s, h) of cloud air at $\hat{p}=60$ mb, while here s_{lc}, h_{sc} of cloud air have been chosen to give saturation at $\hat{p}=65$ mb, and to fit the model. Consequently, the cloud-base mass flux given by Nitta (1975) is larger (about 290 mb day^{-1} rather than 200 mb day^{-1} in Fig. 3). Esbensen (1975) has derived cloud base mass flux from subcloud-layer information and obtained about 245 mb day^{-1} (mean for this 5-day period) at $\hat{p}=60$ mb. This agrees very closely with Fig. 3, extrapolated to 60 mb.

Sarachik (1974) has used the model proposed by Betts (1973a) to derive a cloud-base vertical velocity of the form $(\bar{\omega}-\omega^*)_B$ from the depth of the mixed layer (where $\bar{\omega}_B$ is the large-scale mean vertical motion at cloud base). Sarachik compared this value of ω^*_B with the value derived by Nitta (1975) and concluded that Nitta's value was much too large to permit a mixed layer depth of 500 m ($\hat{p}=56$ mb). However, as pointed out above, ω^* or M_c are parameters derived from and constrained by the more basic convective fluxes (or heating rates), and as such are very sensitive to the choice of level and in-cloud cloud-base properties. For example, decreasing the cloud-base $(s_{lc}-\bar{s})$ given $F_{s_l}(p)$ will increase ω^*_B, but also "detrainment" through $(\partial\omega^*/\partial p)_B$, so that Eqs. (12b) and (14b) are still satisfied. Thus, for a consistent comparison with the mixed layer depth, cloud-base mass flux must be computed from the full Eq. (16) including the detrainment term. Referring to Table 1, we find that just above cloud base, the detrainment term is about one-third of the magnitude of the subsidence term and of opposite sign. The neglect of the detrainment term in Eq. (16) will lead to an estimate of ω^*_B from the depth of the mixed layer of only two-thirds of the "true" value.

Betts (1973a) discussed the maintenance of the stratification in the cumulus layer using a more complex cloud model, which considered both an upward circulation and a reverse downward circulation which resulted after a cloud parcel overshot its first equilibrium level. This conceptual model considered only these two circulations with detrainment to the environment at the parcel's second equilibrium level. A double circulation of this kind was used in that paper as a model to explain why cloud parcels which mix with their environment sometime during their life cycle cannot descend back to cloud base (see Fig. 2 for example), and hence give rise to a downward transport of s_l, which produces the regions of cooling above and warming below shown in Fig. 1. The model used here is a simpler one which only interprets the observed transports (see Table 1), and shows that they are coupled. This simpler model contributes little to an understanding of why the F_{s_l} profile (Fig. 1) has the observed shape. However, in order to show the coupling of the fluxes, the simpler model was necessary because a double circulation (up and down) cannot be uniquely derived from a single flux profile.

8. The problem of interpretation in the precipitation case

Although the main purpose of this paper has been to interpret undisturbed trade-wind budget studies in which precipitation may be neglected, it is useful to consider how much of the methodology can be applied more generally. The vertical flux of liquid water can then no longer be combined as a parcel quantity with the static energy flux or water vapor flux, and Eqs. (8b) and (8c) must be interpreted accordingly with

$$\left.\begin{aligned}\bar{s}_l&=\bar{s}-L\bar{q}_l\\ F_{s_l}&=F_s-F_{Lq_l}\\ F_{Lq}&=F_{Lq_v}+F_{Lq_l}\end{aligned}\right\}.$$

Eq. (8a) is unchanged, and has, therefore, been widely used (e.g., Yanai *et al.*, 1973). The approximations represented by Eq. (9) will still often be valid so that Eqs. (10b), (10c), while still representing the vertical total convective thermal and water fluxes, become

$$F_s-F_{Lq_l}=-\int_0^p (Q_1-Q_R)dp, \tag{18a}$$

$$F_{Lq_v}+F_{Lq_l}=\int_0^p Q_2 dp, \tag{18b}$$

while Eq. (11a) is unchanged. Fig. 7 shows an example of these fluxes derived from Betts (1973b) for a mesoscale cumulonimbus budget over Venezuela. These may be regarded again as the observable convective transports. On this time scale (2 h over land in the late afternoon or early evening) the surface flux of F_h is small compared with the energy flux represented by the surface rainfall which dominates (with opposite sign) in the surface values of $(F_s-F_{Lq_l})$ and $(F_{Lq_v}+F_{Lq_l})$. From the slope of these flux diagrams, it is easy to see the vertical distribution of the drying and warming aloft produced by this surface rainfall.

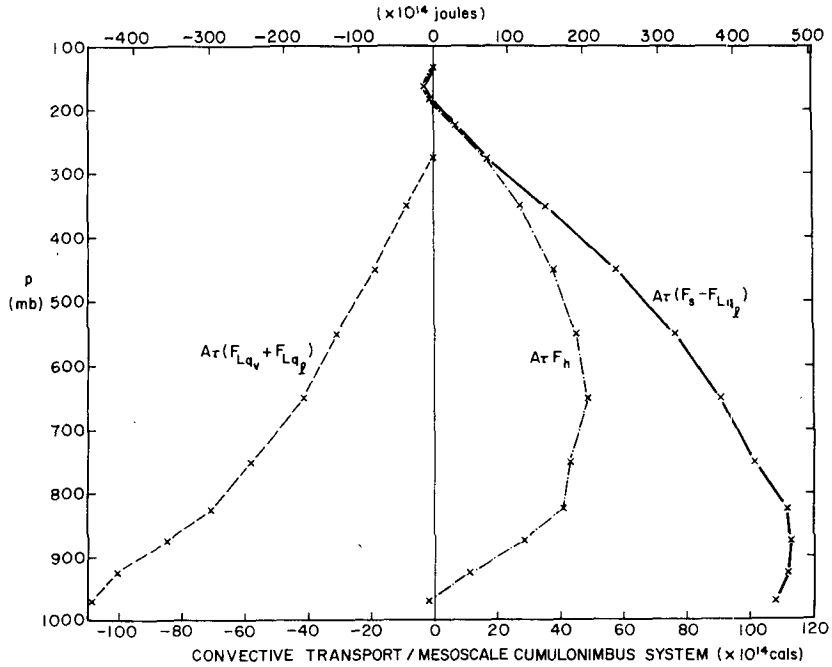

FIG. 7. Total convective transports by one mean mesoscale cumulonimbus system (area $A = 500$ km^2, lifetime $\tau = 2.2$ h) derived from Betts (1973b).

However, further model interpretation of these flux curves requires an adequate model for the vertical structure of the liquid water flux which results from net condensation or evaporation at different levels over the life cycle of the convective system. Even the moist static energy flux cannot, in general, be regarded as independent of the liquid water flux since the evaporation of falling rain is one of the mechanisms for driving the downdrafts which affect F_h [or F_{θ_E}; see Betts (1973b)]. In simple models, however, F_h and F_{Lql} are independent (see Nitta, 1975).

9. Concluding remarks

A simple model has been used to interpret the convective fluxes which one can derive from budget studies of the trade-wind layer. The resulting picture is necessarily dependent on the model chosen, but it seems a useful one. The cloud population can be represented by a cloud mass flux decreasing with height, indicating that in some sense the amount of cloud passing a level decreases with height and becomes near zero at the top (not the bottom) of the trade inversion. Fig. 1 and Table 1 show that while the whole cumulus layer is moistened (detrainment of water from the clouds dominates over the drying effect of cumulus-induced subsidence), the lower part of the layer is warmed and the upper part cooled. The diagnostic model presented here does not explain why this *must* be so. It shows (see Table 1) how this can arise as ω^* decreases and $|s_{lc}-\bar{s}|$ increases. Indeed, since F_{s_l} is always negative in the cloud layer, since $s_{lc}<\bar{s}$, and small near cloud base and at the top of the inversion, it is necessary that a region of warming be balanced by a region of cooling, as discussed in Section 5 and Betts (1973a). However, it is possible for ω^* to decrease so rapidly that F_{s_l} is constant above cloud base and the cumulus have very little thermal effect. This would require a cloud mass flux profile given by

$$\omega^* = \frac{F_{sl}(p_B)}{\bar{s}-s_{lc}}.$$

This profile is a very rapid decrease of ω^* above cloud base which results in the cancellation of the environmental subsidence and detrainment terms in Eq. (14b). The main water vapor input then occurs in a very shallow layer above cloud base. However, in general, the cloud base boundary condition (discussed in Betts, 1973a) requires a region of convective warming above the cloud base to balance that in the subcloud layer, and so maintain the convective stratification against radiative cooling and advective changes. This layer of convective heating requires the downward advection of s_l (or upward advection of q_l) by the mean cumulus field, which results in a cooling of the upper part of the cumulus layer (as shown in Fig. 1). This is the destabilizing process which maintains the trade inversion against the large-scale subsidence. What a non-precipitating cumulus layer cannot do is produce regions of cooling below with warming above. This requires the evaporation of falling precipitation.

The diagnostic study presented here does not *explain* the convective fluxes nor the convective stratification. This paper simply interrelates the convective fluxes and the stratification using a parametric model (Figs. 2, 3 and Table 1). Indeed from the parametric viewpoint, this paper may tend to obscure how the convective transports are controlled, since Q_1, Q_2 and Q_R are derived from large-scale parameters. They may be viewed from the opposite viewpoint, as the fluxes necessary to maintain the convective stratification which is observed to persist with only small changes day after day. From this viewpoint, the fundamental parametric problem is, therefore, what determines the distinctive stratification which we observe to be maintained in the presence of convection. The model proposed by Betts (1973a) attempted to explain the thermal stratification. The model discussed here is a more simple diagnostic one.

However, what this paper has shown is that the thermodynamic transports in the undisturbed trade winds are closely coupled; so that if one derives the thermal convective transports using, for example, a lapse rate adjustment model (as in Betts, 1973a), the water transports are then specified. Alternatively, one may derive the coupled transports simultaneously, as in Arakawa and Schubert (1974), who used a different quasi-equilibrium condition. This paper has also presented a methodology for describing the thermodynamic convective fluxes, using the BOMEX undisturbed period and a VIMHEX budget study as examples; and perhaps clarified further the concepts of entrainment, detrainment and compensating environmental motion which are frequently used in parametric models.

Acknowledgments. This research was supported by the Atmospheric Sciences Section of the National Science Foundation under Grant GA-36323. I would like to thank T. Nitta, S. Esbensen and E. Rasmusson for kindly supplying me with their large-scale budget computations on which this study was based.

REFERENCES

Arakawa, A., and W. Schubert, 1974: Interaction of a cumulus cloud ensemble with the large-scale environment. Part I. *J. Atmos. Sci.*, **31**, 674–701.

Augstein, E., H. Riehl, R. Ostapoff and V. Wagner, 1973: Mass and energy transports in an undisturbed Atlantic trade-wind flow. *Mon. Wea. Rev.*, **101**, 101–111.

Betts, A. K., 1970: Cumulus convection. Ph.D. thesis, Imperial College, University of London, 151 pp.

——, 1973a: Non-precipitation cumulus convection and its parameterization. *Quart. J. Roy. Meteor. Soc.*, **99**, 178–196.

——, 1973b: A composite mesoscale cumulonimbus budget. *J. Atmos. Sci.*, **30**, 597–610.

——, 1974a: Further comments on "A comparison of the equivalent potential temperature and the static energy". *J. Atmos. Sci.*, **31**, 1713–1715.

——, 1974b: The scientific basis and objectives of the U. S. convection subprogram for GATE. *Bull. Amer. Meteor. Soc.*, **55**, 304–313.

, F. J. Dugan and R. W. Grover, 1974: Residual errors of the VIZ radiosonde hygristor as deduced from observations of the sub-cloud layer structures. *Bull. Amer. Meteor. Soc.*, **55**, 1123–1125.

Brunt, D., 1934: *Physical and Dynamical Meteorology*. Cambridge University Press, 411 pp.

Cox, S. K., 1973: Radiation components of the energy budget for BOMEX. Atmos. Sci. Paper No. 208, Colorado State University, Fort Collins, 43 pp.

Esbensen, S., 1975: An analysis of subcloud-layer heat and moisture budgets in the western Atlantic trades. *J. Atmos. Sci.*, **32**; 1921–1923.

Fjelstadt, J., 1925: Graphische Methoden zur Ermittlung adiabatischer Zustandsanderungen feuchter Luft. *Geofys. Publ.*, **3**, No. 13, 25 pp.

Fraedrich, D., 1973: On the parameterization of cumulus convection by lateral mixing and compensating subsidence. Part I. *J. Atmos. Sci.*, **30**, 408–413.

Hoeber, H., 1973: The boundary layer subprogram for the GATE. WMO GATE Report No. 5, 128.

Holland, J. Z., and E. M. Rasmusson, 1973: Measurements of the atmospheric mass, energy and momentum budgets over a 500-kilometer square of tropical ocean. *Mon. Wea. Rev.*, **101**, 44–55.

Kuo, H. L., 1965: On formation and intensification of tropical cyclones through latent heat release by cumulus convection. *J. Atmos. Sci.*, **22**, 40–63.

——, 1974: Further studies on the parameterization of the influence of cumulus clouds on large-scale flow. *J. Atmos. Sci.*, **31**, 1232–1240.

Nitta, T., 1972: Energy budgets of wave disturbances over the Marshall Islands during the years of 1956 and 1958. *J. Meteor. Soc. Japan*, **50**, 71–84.

——, 1975: Observational determination of cloud mass flux distributions. *J. Atmos. Sci.*, **32** (in press).

——, and S. Esbensen, 1974: Heat and moisture budgets using BOMEX data. *Mon. Wea. Rev.*, **102**, 17–28.

Ogura, Y., and H. R. Cho, 1973: Diagnostic determination of cumulus cloud populations from observed large-scale variables. *J. Atmos. Sci.*, **30**, 1276–1286.

Ooyama, K., 1971: A theory on parameterization of cumulus convection. *J. Meteor. Soc. Japan*, **49**, 744–756.

Riehl, H., and J. S. Malkus, 1957: On the heat balance and maintenance of the circulation in the trades. *Quart. J. Roy. Meteor. Soc.*, **83**, 21–29.

Sarachik, E. S., 1974: The tropical mixed layer and cumulus parameterization. *J. Atmos. Sci.*, **31**, 2225–2230.

Yanai, M., S. Esbensen and J. Chu, 1973: Determination of bulk properties of tropical cloud clusters from large-scale heat and moisture budgets. *J. Atmos. Sci.*, **30**, 611–627.